Available online at www.sciencedirect.com
SCIENCE DIRECT®
Journal of the European Ceramic Society 25 (2005) 1073–1079
www.elsevier.com/locate/jeurceramsoc

Self-lubricating behaviors of Al_2O_3/TiB_2 ceramic tools in dry high-speed machining of hardened steel

Deng Jianxin*, Cao Tongkun, Liu Lili

Department of Mechanical Engineering, Shandong University, Jinan 250061, Shandong Province, PR China

Received 9 December 2003; received in revised form 15 March 2004; accepted 26 March 2004
Available online 10 July 2004

Abstract

In this paper, Al_2O_3/TiB_2 ceramic cutting tools with different TiB_2 content were produced by hot pressing. The fundamental properties of these ceramic cutting tools were examined. Dry high-speed machining tests were carried out on hardened steel. The tool wear, the cutting temperature, the cutting forces, and the friction coefficient between the tool and the chip were measured. It was shown that both the wear rates and the friction coefficient at the tool–chip interface of Al_2O_3/TiB_2 ceramic cutting tools in dry high-speed machining of hardened steel were reduced compared with that of in low-speed machining. The mechanisms responsible were determined to be the formation of a self-lubricating oxide film on the tool–chip interface owing to the tribological–chemical reaction by the elevated cutting temperature. The composition of the self-lubricating film was found to be the oxidation product of TiB_2 grains, which serves as lubricating additive on the wear track of the tool rake face. The appearance of this self-lubricating oxide film contributed to the improvement in wear resistance and the decrease of the friction coefficient. This action was even more effective with higher TiB_2 content. Cutting speed was found to have a profound effect on the self-lubricating behavior. In dry low-speed machining of hardened steel, the Al_2O_3/TiB_2 tools showed mainly adhesive and abrasive wear. While in dry high-speed machining, oxidation wear of the ceramic tools was the dominant mechanism due to the very high cutting temperature. No oxide film was formed on the tool–chip interface while machining in nitrogen atmosphere, and the tool wear resistance was correspondingly decreased.

Keywords: Cutting tools; Machining; Cutting; Lubrication; Friction; Al_2O_3; TiB_2

1. Introduction

Machining without the use of any cutting fluid (dry or green machining) is an important objective in industry to reduce environmental and production costs. The advantages of dry machining include:[1–4] non-pollution of the atmosphere or water; no residue on the swarf which will be reflected in reduced disposal and cleaning costs, no danger to health, being non-injurious to skin and allergy free. Moreover, it offers cost reduction in machining. The use of cutting fluids will be increasingly more expensive as stricter enforcement of new standards is imposed, leaving no alternative but to consider dry machining. Dry machining is becoming increasingly popular due to concern regarding the safety of the environment. Recently, consumption of cutting fluids has been reduced considerably by using mist lubrication.[5–7] However, mist in the industrial environment can have serious respiratory effects on the operator.

High-speed machining (HSM) is recognized as one of the key manufacturing technologies for higher productivity and lower production costs.[8–12] The process has been adapted to a wide range of applications. In the aerospace sector, HSM is used to remove large volumes of aluminum quickly and to produce thin walled sections in wings.[12] One of the more recent applications of HSM is in the manufacture of molds and dies from hardened tool steels.[11] Cavities can be produced from solid in the hardened state using HSM, rather than via the more traditional route: machining in the soft condition followed by electrical discharge machining, grinding and hand finishing.

In dry machining, there will be more friction and adhesion between the tool and the workpiece, since they will be subjected to higher temperatures. This will result in increased tool wear and hence reduction in tool life. In high-speed machining, the maximum cutting temperature of the insert involved can reach more than 1000 °C. Conversely, the limit

* Corresponding author.
E-mail address: jxdeng@sdu.edu.cn (D. Jianxin).

0955-2219/$ – see front matter © 2004 Elsevier Ltd. All rights reserved.
doi:10.1016/j.jeurceramsoc.2004.03.033

on cutting speed is a function of the cutting tools used. It was thought that a reduction in all these problems could be achieved by using advanced cutting tool materials to reduce the heat generation by lowering the friction coefficient. The possible strategies involve:[13,14] (1) the isolation of the tool from the workpiece such as introducing a protective layer on the tool face; (2) promoting the transition to the diffusion limited wear regime; (3) picking a tool material chemically stable with respect to the workpiece.

Advances in ceramic processing technology have resulted in a new generation of high performance ceramic cutting tools exhibiting improved properties. Improvements have been made in tool properties such as flexural strength, fracture toughness, thermal shock resistance, hardness, and wear resistance.[15–17]

Alumina is widely used as cutting tool material and it is strengthened by the addition of particles like zirconium oxide (ZrO_2), titanium carbide (TiC), silicon carbide whiskers (SiC_w), titanium boride (TiB_2), and titanium nitride (TiN) to improve the properties. The strengthening or the toughening mechanisms of these ceramic composites are phase transformation toughening, whisker toughening and precipitate or dispersion strengthening.[18,19] These developments have now enabled ceramic tools to be used in the machining of various types of steel, cast iron, non-ferrous metals, and refractory nickel based alloys at very high-speed.[17,20,21] Thus, the productivity is improved by shorter cycle times, and the cost of manufacturing is reduced.

Now ceramic cutting tools are applied widely for machining hard materials in industry due to their unique mechanical properties. In most cases, the machining is conducted under dry or high-speed conditions, which causes high cutting temperature, high friction coefficient and wear rate, especially when cutting some difficult-to-cut materials like hardened steel. In this study, Al_2O_3/TiB_2 ceramic cutting tools with different TiB_2 content were produced by hot pressing. The fundamental properties of these ceramic cutting tools were examined. Dry high-speed machining tests were carried out on the hardened steel with these ceramic tools. The tool wear, the cutting temperature, the cutting forces, and the friction coefficient between the tool and the chip were measured. The wear mechanisms of these tools were investigated and correlated to the oxide film formed on the tool–chip interface owing to the tribological–chemical reaction. The purpose was to characterize the self-lubrication behaviors of Al_2O_3/TiB_2 ceramic cutting tools during dry high-speed machining.

2. Materials and experimental procedures

2.1. Preparation of Al_2O_3/TiB_2 ceramic cutting tools

The average particle size of the $A1_2O_3$ and TiB_2 source powders is less than 2.0 μm, and the combinations are listed in Table 1. The combined powders were prepared by wet ball milling in alcohol with cemented carbide balls for 100 h. Following drying, the powdered material was formed and compacted in a metal die with a pressure of 60 MPa. Following the forming stage, the compacted powders was then filled in a graphite die, and the final densification was accomplished by hot pressing with a pressure of 36 MPa in nitrogen atmosphere for 20–60 min to produce a disk. The required sintering temperature was in the range of 1650–1800 °C. Details of these procedures and specific processing parameters employed are described elsewhere.[22,23]

Densities of the hot-pressed materials were measured by the Archimedes's method. Test pieces of 3 mm × 4 mm × 36 mm were prepared from the hot-pressed disks by cutting and grinding using a diamond wheel[22] and were used for the measurement of flexural strength, Vickers hardness and fracture toughness. A three-point bending mode was used to measure the flexural strength over a 30 mm span at a crosshead speed of 0.5 mm/min. Fracture toughness measurement was performed using indentation method in a hardness tester (ZWICK3212) using the formula proposed by Cook and Lawn.[24] On the same apparatus the Vickers hardness was measured on the polished surface with a load of 98 N. Data for flexural strength, hardness and fracture toughness were gathered on five specimens.

2.2. Cutting tests

Cutting tests were carried out on a CA6140 lathe equipped with a commercial tool holder having the following geometry: rake angle $\gamma_o = -5°$, clearance angle $\alpha_o = 5°$, inclination angle $\lambda_s = -5°$, side cutting edge angle $K_r = 75°$. The geometry of the Al_2O_3/TiB_2 tool inserts was of ISO SNGN150608 with a 0.2 mm at 20° edge chamfer. The workpiece material used was $45^{\#}$ hardened steel with a hardness of HRC45–50 in the form of round bar with an external di-

Table 1
Mechanical properties of Al_2O_3/TiB_2 ceramic tools with different TiB_2 content

Sample	Composition (vol.%)		Relative density (%)	Fracture toughnes ($MPa\,m^{1/2}$)	Flexural strength (MPa)	Hardness (GPa)
	$A1_2O_3$	TiB_2				
AB10	90	10	99.9	3.7	650	19.6
AB20	80	20	99.7	4.7	775	20.1
AB30	70	30	99.2	5.2	785	20.8
AB40	60	40	98.5	4.9	670	21.3

ameter of 150 mm. No cutting fluid was used in the machining processes. Nitrogen and air atmosphere were used to investigate the effect of various atmosphere on the tool wear behaviors under similar conditions. All tests were carried out with the following parameters: depth of cut $a_p = 0.4$ mm, feed rates $f = 0.15$ mm/r, cutting time $t = 12$ min.

Tool flank wear was measured using a 20× optional microscope system linked via transducers to a digital read out. Cutting forces were obtained with a KISTLER piezoelectric quartz dynamometer linked via change amplifiers to a chart recorder. The average cutting temperature of the tool rake face was measured by means of nature thermocouple technique.[25] The worn rake and flank regions on the ceramic tools were examined using scanning electron microscopy (SEM). The elemental chemical composition of the worn areas was determined by X-ray diffraction analysis.

3. Results and discussions

3.1. Mechanical properties and microstructural characterization of Al_2O_3/TiB_2 ceramic tools

Results of the fracture toughness, flexural strength, hardness and relative density of Al_2O_3/TiB_2 ceramic tool materials with different content of TiB_2 are presented in Table 1. It was shown that the fracture toughness increase with increasing TiB_2 content up to 30 vol.% and slightly decreased at 40 vol.%, the trend of the flexural strength being the same as that of the fracture toughness. However, the specimen with higher TiB_2 content showed higher hardness, and the hardness increased with increasing TiB_2 content up to 40 vol.%.

The SEM micrograph of the fracture surface of Al_2O_3/TiB_2 (AB30) ceramic tool material was shown in Fig. 1. As can be seen that Al_2O_3/TiB_2 composite exhibited a rough fracture surface and showed signs of longer crack deflection path. The fracture mode was mixed transgranular and intergranular. Fig. 2 shows typical backscattered electron image of Al_2O_3/TiB_2 (AB30) ceramic tool material. Polished surface of the ceramic specimens were etched using a hot-solution of phosphoric acid for five hours. In this structure, the white phases with clear contrast are TiB_2 and the grey phases are $A1_2O_3$. It is indicated that porosity is virtually absent, and the second phases were uniformly distributed with the matrix, and there were few second phases agglomerates or matrix-rich regions.

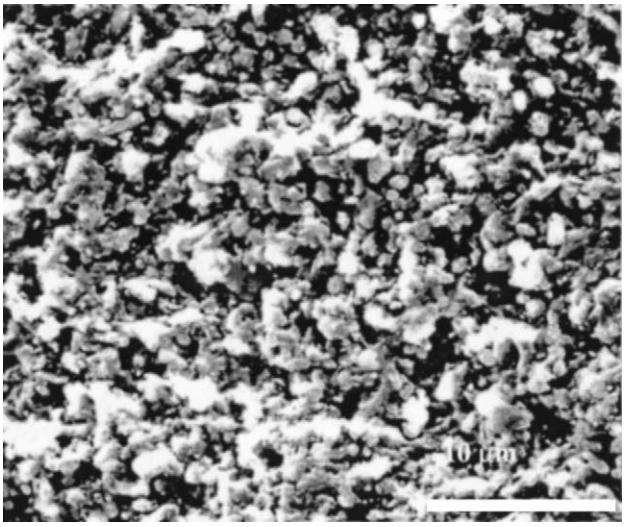

Fig. 1. SEM micrograph of the fracture surface of Al_2O_3/TiB_2 (AB30) ceramic tool material.

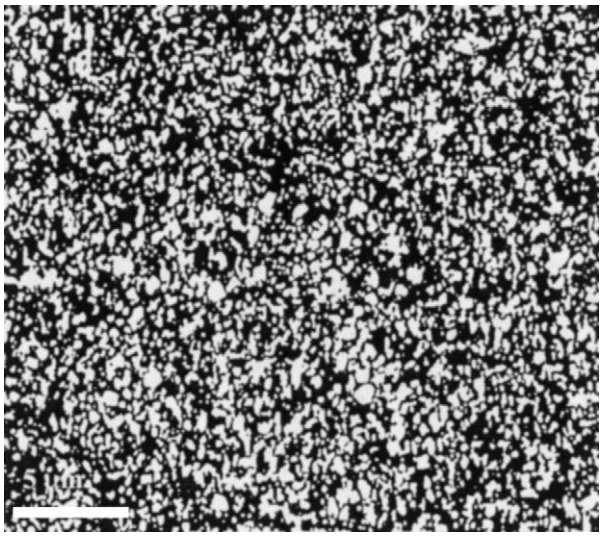

Fig. 2. Typical back scattered electron image of Al_2O_3/TiB_2 (AB30) ceramic tool material.

3.2. Cutting performance and self-lubricating behaviors of TiB_2 strengthening Al_2O_3 ceramic tools with different TiB_2 content

Fig. 3 shows the flank wear of Al_2O_3/TiB_2 ceramic tools with different TiB_2 content when dry machining hard-

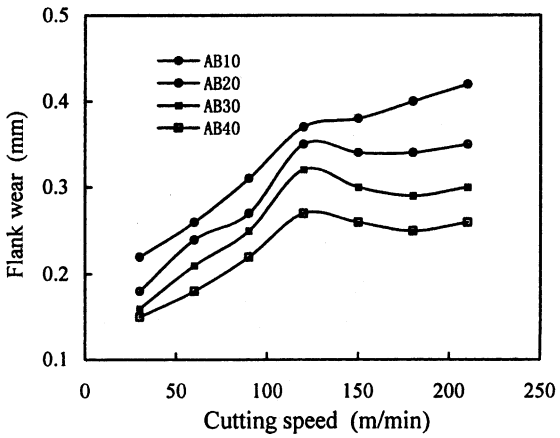

Fig. 3. Effect of TiB_2 content and cutting speed on the flank wear of Al_2O_3/TiB_2 tool in dry machining of hardened steel (test conditions: depth of cut $a_p = -0.4$ mm, feed rates $f = 0.15$ mm/r, cutting time $t = 12$ min).

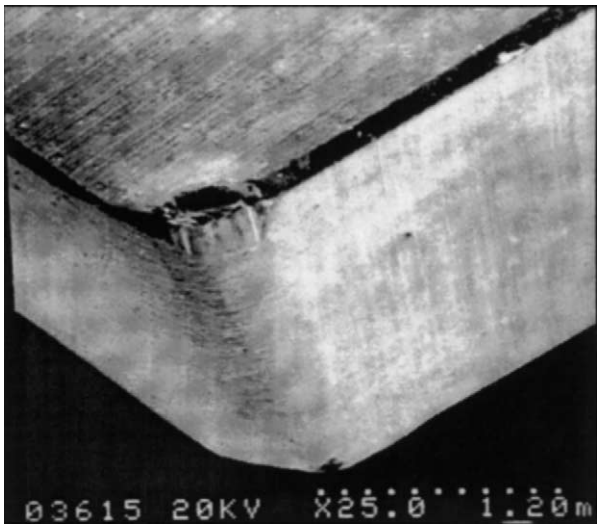

Fig. 4. SEM micrograph of the wear profile of Al_2O_3/TiB_2 (AB30) ceramic cutting tool (test conditions: cutting speed $v = 60$ m/min, depth of cut $a_p = 0.4$ mm, feed rates $f = 0.15$ mm/r, cutting time $t = 12$ min).

ened steel at different cutting speeds. It can be seen that the flank wear of these ceramic tools increased very fast up to cutting speeds of 120 m/min, followed by downward trend (with the exception of AB10). This action was even more effective with higher TiB_2 content. The ceramic tools with higher TiB_2 content showed more wear resistance.

Fig. 4 shows the SEM micrograph of the wear profile of Al_2O_3/TiB_2 (AB30) ceramic tool when the cutting speed was 60 m/min. It appears that both the rake face and flank face were severely worn under these test conditions. Fig. 5 shows SEM micrographs of the crater wear and flank wear track of Al_2O_3/TiB_2 (AB30) ceramic tool, respectively. It can be seen that there were many mechanical plowing grooves on the worn flank face, and it was indicative of typical abrasive wear. While on the worn rake face, serious adhesive wear can be clearly seen.

The crater depth profiles of Al_2O_3/TiB_2 (AB30) ceramic tool obtained at different cutting speeds and atmosphere are illustrated in Fig. 6. It was shown that the crater wear profiles of Al_2O_3/TiB_2 ceramic tool are different when machining in air and nitrogen atmosphere. The crater depth increased gradually when cutting in nitrogen atmosphere. While in air atmosphere, Al_2O_3/TiB_2 ceramic tool showed wider and deeper crater wear at cutting speed lower than 100 m/min, and exhibited very small crater wear at cutting speed higher than 150 m/min. No obvious crater wear was developed on the rake face at a cutting speed of 210 m/min.

Fig. 7 shows the cutting temperatures of Al_2O_3/TiB_2 ceramic tool as a function of cutting speeds in dry machining of hardened steel. It was found that the cutting temperature increased exponentially with increasing cutting speeds. The cutting temperature is higher than 800 °C when the cutting speed is above 120 m/min, and 1190 °C up to cutting speed of 210 m/min. Under such high cutting temperature, the TiB_2 of the ceramic tool material may be oxidized. The oxidation reaction can be described as the following formula:[26,27]

$$2TiB_2 + 5O_2 \rightarrow 2TiO_2 + 2B_2O_3 \quad (1)$$

According to Eq. (1), the oxidation products of TiB_2 grain are composed of phases of TiO_2 and B_2O_3. The X-ray diffraction analysis of Al_2O_3/TiB_2 ceramic tool before and after cutting at 210 m/min, showed the presence of TiO_2 on the wear track, as shown in Fig. 8. No B_2O_3 is observed on the wear track because of the vaporizing due to its low melting point (about 570 °C). The SEM micrograph of the worn rake face of Al_2O_3/TiB_2 ceramic tool in dry machining of hardened steel at a cutting speed of 210 m/min in air atmosphere is shown in Fig. 9. In comparison with Fig. 5, it exhibited a relative smooth surface, both mechanical plowing grooves and adhesion could not be observed, and there

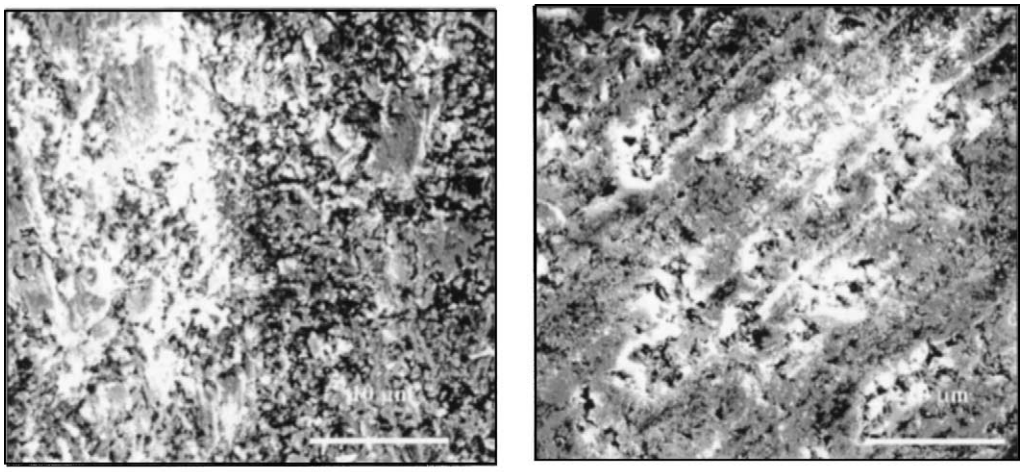

(a) Crater wear (b) Flank wear

Fig. 5. SEM micrographs of the crater wear and flank wear area of Al_2O_3/TiB_2 (AB30) ceramic cutting tool (test conditions: cutting speed $v = 60$ m/min, depth of cut $a_p = 0.4$ mm, feed rates $f = 0.15$ mm/r, cutting time $t = 12$ min).

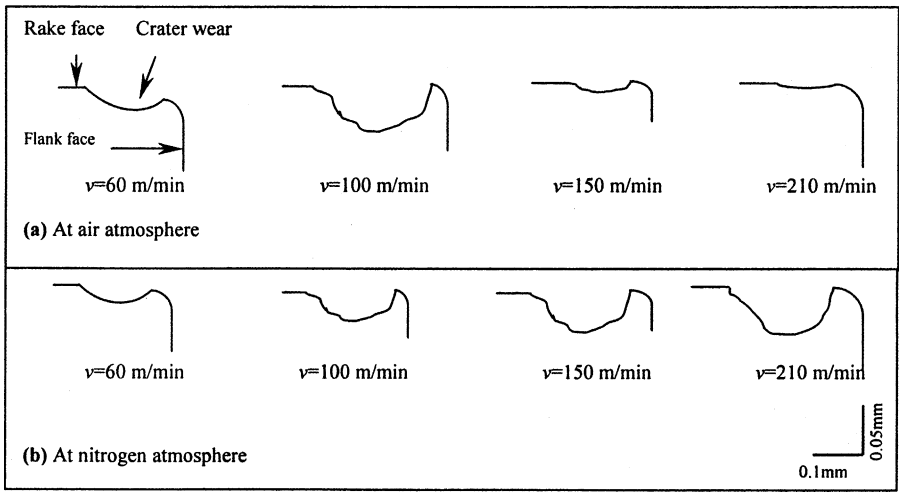

Fig. 6. Schematic diagram of the crater wear profiles of Al_2O_3/TiB_2 (AB30) ceramic cutting tool at different atmosphere and cutting conditions.

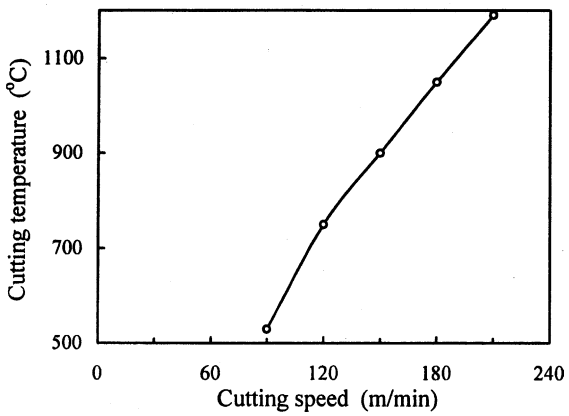

Fig. 7. Effect of cutting speed on the cutting temperature of Al_2O_3/TiB_2 ceramic tool in dry machining of hardened steel (test conditions: depth of cut $a_p = 0.4$ mm, feed rates $f = 0.15$ mm/r, cutting time $t = 12$ min).

is no distinct crack on the wear track. Fig. 10 gives SEM micrograph of the cross-sectional views of Al_2O_3/TiB_2 ceramic tool in dry machining of hardened steel at a cutting speed of 210 m/min in air atmosphere. It is clearly that there is a thin film on the wear track. The thickness of this film is about 2–4 μM. It was found that this thin film was created by the oxidation of TiB_2.

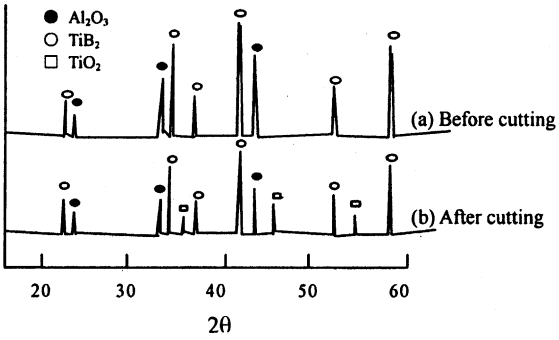

Fig. 8. The X-ray diffraction patterns of Al_2O_3/TiB_2 ceramic tool before and after cutting at 210 m/min.

The friction coefficient between two smooth bodies sliding under elasticity loaded conditions in an elliptical contact can be decreased as:[28]

$$\mu = A\frac{\tau}{P^{1/3}}\left(\frac{3}{4E'}\right)^{2/3} \quad (2)$$

where A is a constant determined by contact geometry; τ, critical shear stress at the interface, which may be an oxide film; P, normal load, and E', effective elastic modulus of the contact materials.

For a given contact geometry Eq. (2) shows that the friction coefficient varies linearly with critical shear stress. When there is an oxide film on the wear surface, the matrix endures the load, and friction occurs on the oxide film.[29,30] As the oxide film on the wear surface had a much smaller critical shear stress than the substrate and thus resulted in a reduced friction coefficient according to Eq. (2) when dry

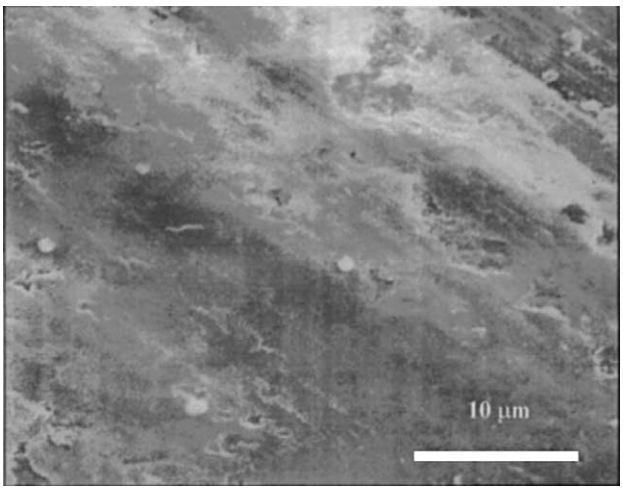

Fig. 9. SEM micrograph of the worn rake face of Al_2O_3/TiB_2 ceramic tool in dry machining of hardened steel in air atmosphere (test conditions: cutting speed $v = 210$ m/min, depth of cut $a_p = 0.4$ mm, feed rates $f = 0.15$ mm/r, cutting time $t = 12$ min).

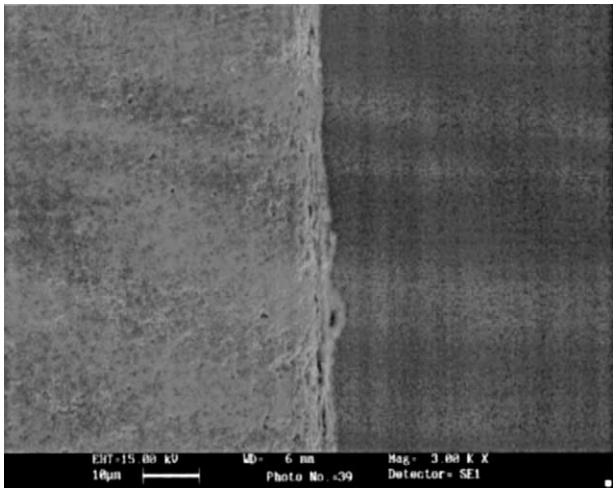

Fig. 10. Cross-sectional view SEM micrograph of the worn rake face of Al_2O_3/TiB_2 ceramic tool in dry machining of hardened steel in air atmosphere (test conditions: cutting speed $v = 210$ m/min, depth of cut $a_p = 0.4$ mm, feed rates $f = 0.15$ mm/r, cutting time $t = 12$ min).

high-speed machining of hardened steel. This means that the oxide film on the tool rake face acted as lubricant. Thus, self-lubrication can be accomplished under these conditions.

The friction coefficient between the tool and the chip interface could be calculated based on the following formula:[25]

$$\mu = \tan(\beta) = \tan\left(\gamma_o + \arctan\left(\frac{F_r}{F_z}\right)\right) \quad (3)$$

where β is the friction angle; γ_o, rake angle; F_r, radial force; F_z, main cutting force.

Fig. 11 illustrates the friction coefficient between the tool–chip interface of Al_2O_3/TiB_2 ceramic tool with different TiB_2 content as a function of cutting speeds in dry machining of hardened steel. It was found that the friction coefficient showed a downward trend with the increasing of the cutting speeds. The ceramic tools with higher TiB_2 content showed lower friction coefficient under the same

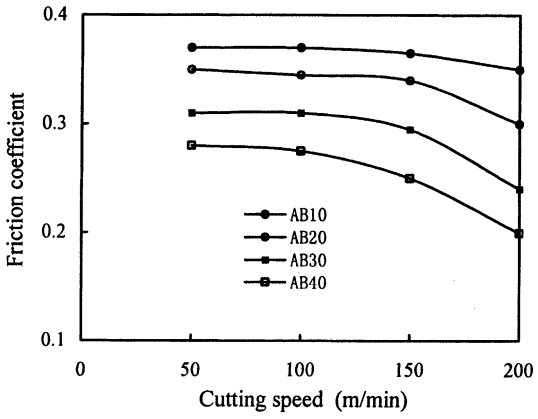

Fig. 11. Effect of cutting speed on the friction coefficient between the tool and the chip of Al_2O_3/TiB_2 ceramic tool in dry machining of hardened steel (test conditions: depth of cut $a_p = 0.4$ mm, feed rates $f = 0.15$ mm/r, cutting time $t = 12$ min).

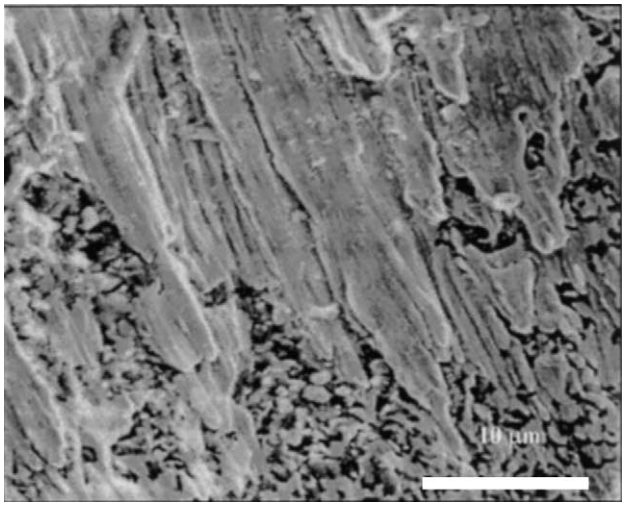

Fig. 12. SEM micrograph of the worn rake face of Al_2O_3/TiB_2 ceramic tool in dry machining of hardened steel in nitrogen atmosphere (test conditions: cutting speed $v = 210$ m/min, depth of cut $a_p = 0.4$ mm, feed rates $f = 0.15$ mm/r, cutting time $t = 12$ min).

test conditions. The friction coefficient kept almost constant at low cutting speeds (smaller than 150 m/min), and within further increasing of the cutting speed the friction coefficient decreased gradually. This action was even more effective with higher TiB_2 content. This may be explained by the oxide film formed on the tool rake face owing to the tribological–chemical reaction by the elevated cutting temperature. Therefore, formation of the lubricious oxide film on the wear surface resulted in a decrease in friction coefficient and wear rates. Oxidation wear of the ceramic tools was the dominant wear mechanism in dry high-speed machining hardened steel due to the very high cutting temperature.

The SEM micrograph of the worn rake face of Al_2O_3/TiB_2 ceramic tool in dry machining of hardened steel at speed of 210 m/min in nitrogen atmosphere is shown in Fig. 12. It can be seen that Al_2O_3/TiB_2 ceramic tool exhibited serious adhesion wear on the rake face. Nitrogen was found to have obvious effect on the tool wear because it is easy for nitrogen to enter into the tool–chip interface. The nitrogen in the tool–chip interface prohibited the oxidation of the TiB_2, no lubricious oxide film was formed, and this was found to be responsible for the decreasing of wear resistance of Al_2O_3/TiB_2 ceramic tool under this test conditions.

4. Conclusions

Al_2O_3/TiB_2 ceramic cutting tools with different TiB_2 content were produced by hot pressing. Dry high-speed machining tests were carried out on hardened steel. Results showed that:

1. Both the wear rates and the friction coefficient between the tool and chip interface of TiB_2 strengthening Al_2O_3

ceramic tools were reduced in dry high-speed machining of hardened steel. The mechanisms responsible were determined to be the formation of a self-lubricating oxide film on the tool–chip interface owing to the tribological–chemical reaction by the elevated cutting temperature.

2. The composition of the self-lubricating film was found to be the oxidation product of TiB_2 grains, which serves as lubricating additive. The appearance of this self-lubricating oxide film on the wear track contributed to the improvement in wear resistance and decrease of the friction coefficient. This action was even more effective with higher TiB_2 content.
3. Cutting speed was found to have a profound effect on the self-lubricating behavior of these ceramic tools during dry high-speed machining processes. In dry low-speed machining of hardened steel, the Al_2O_3/TiB_2 tools showed mainly adhesive and abrasive wear. While in dry high-speed machining, oxidation wear of the ceramic tools was the dominant mechanism due to the very high cutting temperature.
4. No oxide film was formed on the tool–chip interface while machining in nitrogen atmosphere, and the tool wear resistance was correspondingly decreased.

Acknowledgements

This work was supported by “the National Natural Science Foundation of China (50275088)”, “the Excellent Young Teachers Program of MOE (2055)”, and “the Scientific Research Foundation for the Excellent Young Scientists of Shandong Province (02BS064)”.

References

1. Klocke, F. and Eisenblatter, G., Dry cutting. *Ann. CIRP* 1997, **46**(2), 519–526.
2. Sreejith, P. S. and Ngoi, B. K. A., Dry machining: machining of the future. *J. Mater. Process. Technol.* 2000, **101**, 287–291.
3. Kustas, F. M., Fehrehnbacher, L. L. and Komanduri, R., Nanocoatings on cutting tool for dry machining. *Ann. CIRP* 1997, **46**(1), 39–42.
4. Narutaki, N., Yamane, Y., Tashima, S. and Kuroki, H., A new advanced ceramic for dry machining. *Ann. CIRP* 1997, **46**(1), 43–48.
5. Klocke, F., Krieg, T. and Lugscheider, E., Testing and design of tool coatings with properties adapted to the use of biodegradable cutting fluids. *Ann. CIRP* 2001, **50**(1), 57–60.
6. Braga, U. D., Diniz, A. E. and Miranda, G. W. A., Using a minimum quantity of lubricant (MQL) and a diamond coated tool in the drilling of aluminum–silicon alloys. *J. Mater. Process. Technol.* 2002, **122**(1), 127–138.
7. Rahman, M., Senthil Kumar, A. and Salam, M. U., Experimental evaluation on the effect of minimal quantities of lubricant in milling. *Int. J. Machine Tools Manuf.* 2002, **42**(5), 539–547.
8. Herbert, S., High-speed machining. *Ann. CIRP* 1992, **41**(2), 637–645.
9. Sandstrom, D. R. and Hodowany, J. N., Modeling the physics of metal cutting in high-speed machining. *Mach. Sci. Technol.* 1998, **22**, 343–353.
10. Dolinsek, S., Sustarsic, B. and Kopac, J., Wear mechanisms of cutting tools in high-speed cutting processes. *Wear* 2001, **250/251**, 349–356.
11. Dewes, R. C. and Aspinwall, D. K., A review of ultra high speed milling of hardened steels. *J. Mater. Process. Technol.* 1997, **69**, 1–17.
12. Ezugwu, E. O., Bonney, J. and Yamane, Y., An overview of the machinability of aeroengine alloys. *J. Mater. Process. Technol.* 2003, **134**(2), 233–253.
13. Jianxin, D., Xing, A. and Yihua, F., Wear, lubrication and matching of cutting tools with the workpiece materials. *Chin. J. Mech. Eng.* 2002, **38**(4), 40–45.
14. Klocke, F. and Krieg, T., Coated tools for metal cutting features and applications. *Ann. CIRP* 1999, **48**(2), 515–525.
15. Brandt, G., Ceramic cutting tools, state of the art and development trends. *Mater. Technol.* 1999, **14**(1), 17–22.
16. Whitney, E. D., Microstructural engineering of ceramic cutting tools. *Ceram. Bull.* 1988, **67**(6), 1010–1015.
17. Xing, A., Zhaoqian, L. and Jianxin, D., Development and perspective of advanced ceramic cutting tool materials. *Eng. Mater.* 1995, **108**, 53–66.
18. Evans, A. G., Perspective on the development of high toughness ceramics. *J. Am. Ceram. Soc.* 1990, **73**(2), 187–195.
19. Steinbrech, R. W., Toughening mechanisms for ceramic materials. *J. Eur. Ceram. Soc.* 1992, **8**(10), 131–137.
20. Brandt, G., Gerendas, A. and Mikus, M., Wear mechanisms of ceramic cutting tools when machining ferrous and non-ferrous alloys. *J. Eur. Ceram. Soc.* 1990, **6**(5), 273–290.
21. Jianxin, D. and Xing, A., Wear behavior and mechanisms of alumina based ceramic tools in machining of ferrous and non-ferrous alloys. *Tribol. Int.* 1997, **30**(11), 807–813.
22. Jianxin, D., *Development of TiB_2 Reinforced Alumina Based Ceramic Tool Materials and Study on its Friction and Wear Behaviours*. Ph.D. dissertation, Shandong University of Technology, 1995.
23. Jianxin, D. and Xing, A., Friction and wear behavior of Al_2O_3/TiB_2 ceramic composite against cemented carbide in various atmosphere at elevated temperature. *Wear* 1996, **195**, 128–132.
24. Cook, R. F. and Lawn, B. R., A modified indentation toughness technique. *J. Am. Ceram. Soc.* 1983, **66**(11), C-200–C-201.
25. Cheng, R., *Principle of Metal Cutting*. China Machine Press, Beijing, 1992.
26. Matsushita, J. and Hayashi, S., Oxidation of TiB_2/Al_2O_3 composites in air. *J. Ceram. Soc. Jpn.* 1990, **98**, 323–326.
27. Jianxin, D. and Xing, A., Effect of TiB_2 particle and SiC whisker additions on the friction and wear behaviors of Al_2O_3 ceramic. *J. Adv. Mater.* 1996, **27**(4), 32–36.
28. Liu, H. and Fine, M., Tribological behavior of SiC whisker/Al_2O_3 composites against carburized 8620 steel in lubrication sliding. *J. Am. Ceram. Soc.* 1991, **74**(9), 2224–2233.
29. Page, R. A., Development of self-lubricating ceramics using surface and bulk oxidizing species. In *Advances in Engineering Tribology*. STLE Publication, Illinois, 1991.
30. Sliney, H. E., Solid lubrication materials for high temperatures—a review. *Tribol. Int.* 1982, **15**, 303–314.